

www.acsami.org Research Article

Vat Photopolymerization Additive Manufacturing of Tough, Fully **Recyclable Thermosets**

Alexa S. Kuenstler, Juan J. Hernandez, Marianela Trujillo-Lemon, Alexander Osterbaan, and Christopher N. Bowman*

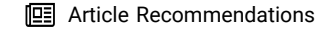


Cite This: ACS Appl. Mater. Interfaces 2023, 15, 11111–11121



ACCESS I

III Metrics & More



Supporting Information

ABSTRACT: To advance the capabilities of additive manufacturing, novel resin formulations are needed that produce high-fidelity parts with desired mechanical properties that are also amenable to recycling. In this work, a thiol-ene-based system incorporating semicrystallinity and dynamic thioester bonds within polymer networks is presented. It is shown that these materials have ultimate toughness values >16 MJ cm⁻³, comparable to high-performance literature precedents. Significantly, the treatment of these networks with excess thiols facilitates thiol—thioester exchange that degrades polymerized networks into functional oligomers. These oligomers are shown to be amenable to repolymerization into constructs with varying thermomechanical properties, including elastomeric networks that recover their shape fully from >100% strain. Using a commercial stereolithographic printer, these resin formulations are printed into functional objects including both stiff ($E \sim 10-100 \text{ MPa}$) and soft ($E \sim 1-10 \text{ MPa}$) lattice structures. Finally, it is shown that the incorporation of both dynamic chemistry and crystallinity further enables advancement in the



properties and characteristics of printed parts, including attributes such as self-healing and shape-memory.

KEYWORDS: polymers, photopolymerization, additive manufacturing, recycling, dynamic chemistry

1. INTRODUCTION

Additive manufacturing has emerged as a powerful method to assemble soft matter into objects rapidly and precisely with properties and geometries often inaccessible using traditional techniques. While numerous additive techniques for polymeric systems have been developed, 1,2 vat photopolymerizationbased 3D printing is particularly attractive due to its ability to fabricate micrometer-scale features through simple low-cost stereolithographic (SLA) or digital light projection (DLP) hardware and high-efficiency light-emitting diodes (LEDs).3 The resins used in these systems typically contain multifunctional monomers or oligomers that form crosslinked networks (i.e., thermosets) upon photopolymerization, where layer-bylayer projections of patterned light control the overall geometry of the final object. While crosslinking increases the modulus and dimensional stability of printed objects, other critical mechanical properties such as extensibility and toughness are often compromised. This approach significantly limits the accessible material property space, particularly as compared to extrusion-based additive manufacturing such as fused deposition modeling and direct ink writing approaches which are compatible with diverse polymeric systems such as tough thermoplastics, 5-9 soft gels, 10-12 and stiff composites that often incorporate semicrystalline materials. 13-15 Furthermore, the thermosets overwhelmingly produced in vat photopolymerization are intractable, cannot be reprocessed or recycled, and possess little capacity for healing or mending. This behavior ultimately introduces significant sustainability

concerns particularly in fields such as rapid prototyping where objects are produced and disposed of at high rates.

One method to preserve the ambient performance of thermosets while facilitating reprocessing and recycling under specific conditions is through the inclusion of dynamic covalent bonds (DCBs). These covalent bonds undergo chemical exchange reactions when activated by stimuli such as heat, 19-23 chemical catalysts, 24-28 and light. 29-31 When static crosslinking functionalities are replaced with DCBs, these moieties preserve network structure and performance until a stimulus is introduced, where subsequent bond exchange facilitates polymer chain rearrangement and network plasticity. The chemical details, exchange mechanism, and stoichiometry of a particular DCB system can be tuned to access diverse behaviors ranging from full network relaxation for remolding,^{32,33} interfacial reactions for self-healing,³⁴ and backbone scission to revert to oligomers.^{35,36} Even though several DCB systems have been incorporated in bulk photopolymers, they have been sparsely employed in DLP-based 3D printing to date. However, existing examples demonstrate the powerful ability of dynamic covalent chemistry to be used as a tool to

Received: December 12, 2022 Accepted: February 8, 2023 Published: February 16, 2023





modulate materials in time and space, including enhanced interlayer adhesion, 37 postprinting modification, $^{38-40}$ and life cycle control.41-44

To further extend DCB use in light-based additive manufacturing, resin systems that are compatible with photopolymerization and readily incorporate dynamic monomers are needed. Thiol-ene photopolymerization is a particularly promising synthetic method in this regard because it facilitates high monomer conversion on short timescales $(\approx 1-10 \text{ s})$, is highly oxygen tolerant for use under ambient conditions, and demonstrates low shrinkage stress for high-fidelity and low-warp printing of large areas. 45–50 Furthermore, several dynamic monomers are easily incorporated into thiolene reactions, including thioesters, 51,52 anhydrides, 53 and disulfides.⁵⁴ Despite these advantages, it remains a challenge to realize desired mechanical properties such as stiffness, elongation, and toughness in thiol-ene or other single-stage vat photopolymerization processes. The most common strategy to synergistically improve mechanical performance is to incorporate urethane^{55–57} or triazole⁵⁸ linkages for hydrogen-bonding-induced energy dissipation. However, these associative interactions also increase the resin viscosity,⁵⁹ which is often detrimental to printing performance. An alternative approach to improve mechanical performance without increasing resin viscosity is through crystallization. Our group recently introduced a method to produce lightly crosslinked semicrystalline networks, 60 where self-assembly of the network into crystalline lamellae was shown to produce both thermoplastic-like extensibility and toughness, while covalent crosslinks endow these materials with increased stiffness and dimensional stability. However, while crystalline thermoplastics find widespread use due to their favorable mechanical properties and ability to be reprocessed upon melting at elevated temperatures, crosslinked analogues cannot be reconfigured.

To realize 3D printed parts that combine both superior mechanical performance and amenability to recycling and reprocessing, DCBs were incorporated within semicrystalline networks. In this work, tough and dynamic networks are reported that can be degraded and repolymerized for sustainable and high-performance 3D printed parts. Specifically, we show that thioester groups incorporated within thiolene networks result in diverse mechanical properties ranging from tough, thermoplastic-like semicrystalline materials to soft, amorphous elastomers that are comparable to previously reported vat photopolymerization resins. However, unlike traditional printing resins, it is demonstrated that thiolthioester exchange reactions facilitate triggerable reversion into functional oligomers that are subsequently repolymerized while conserving thermomechanical properties. These materials are printed using a commercially available SLA printer to produce parts that are chemically recyclable over several cycles. Additionally, it is demonstrated that printed parts of different compositions are degraded into chemically similar building blocks for "single-stream" recycling into new printed parts. Last, the unique thermomechanical properties of these networks, achieved by combining covalent network formation, crystallinity, and dynamic bonds, are used to facilitate advanced capabilities such as shape memory and self-healing, thus considerably expanding the toolbox of functional SLAprinted parts.

2. RESULTS AND DISCUSSION

2.1. Preparation and Characterization of Semicrystalline Networks. Dynamic networks were prepared through the photopolymerization of aliphatic dithiol 1,10-decanedithiol (DDT), the tetrathiol crosslinker pentaerythritol tetrakis(3mercaptopropionate) (PETMP), and a thioester diallyl ether monomer (TEDA), with a 1 mol % 2,4,6-trimethylbenzoyldiphenyl phosphine oxide (TPO) photoinitiator under 405 nm light (Scheme 1). The kinetics and material property

Scheme 1. Monomers and Network Structure

development of these networks were studied using real-time Fourier transform infrared (FTIR) spectroscopy and in situ photorheology, as shown in Figure 1 for a representative composition of 1:1.05 allyl ether/thiol with 5:95 molar ratio PETMP/DDT (the significance of this formulation will be discussed later). Samples were observed to gel into a crosslinked network within several seconds upon illumination with 405 nm light (\approx 10 mW cm⁻², 5 min), as evidenced by the crossover of G'/G'' and concurrent consumption of functional groups (Figure 1A). Additionally, materials of sufficiently low crosslink density showed an increase in shear modulus over longer times. The stiffening of the network is caused by crystallization, as shown by differential scanning calorimetry (DSC), which displays two melting temperatures (T_m) of 36.0 and 46.5 °C with a combined melting enthalpy ($\Delta H_{\rm m}$) of 44.7 J g⁻¹ (Figure 1B). This behavior is further corroborated by no change in FTIR spectra over the experimental time frame (Figure S1), providing further evidence that the modulus increase is due to crystallization and not additional crosslinking or other chemical reactions.

The properties of step growth networks are readily tuned through simple alteration of either the reactive group stoichiometry or the equivalent weight per functional group in the monomer, particularly for ternary monomer combinations such as those explored here. Thus, initial studies were conducted to screen the effect of the stoichiometric ratio of allyl ether/thiol and dithiol/tetrathiol on morphological, thermal, and mechanical properties (Tables S1-S4). Two general trends were observed. First, as more excess thiol is introduced to the network, crystallinity increased, but the films fractured at lower strains, likely due to the simultaneous decrease in crosslink density and the introduction of defects into the network structure. 61,62 Second, as the amount of the tetrathiol crosslinker was decreased, crystallinity increased in addition to extensibility, leading to tougher films. Using this

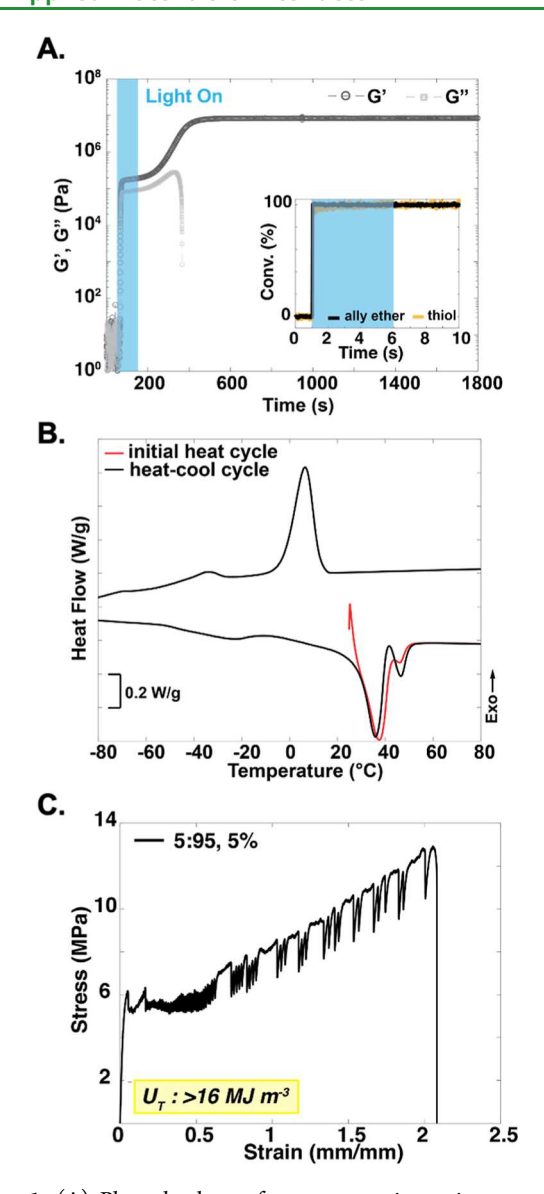


Figure 1. (A) Photorheology of a representative resin composition shows gelation, followed by crystallization and full monomer conversion (FTIR, inset). (B) DSC shows sample crystallinity. (C) Tensile test of the network reveals a stiff and extensible network with high toughness.

system, semicrystalline networks were accessed with moduli E = 210 \pm 22 MPa and ultimate toughness values (U_T) = 16.1 \pm 1.8 MJ m⁻³ for films (Figure 1C) containing 1:1.05 allyl ether/ thiol with a 5:95 ratio of DDT/PETMP (herein referred to as the "tough" composition and used for the majority of subsequently discussed studies). We note that the saw-like features in the stress-strain curves have been previously observed⁶⁰ and likely arise due to plastic instabilities as crystalline lamellae are pulled apart, 63 thus providing a mechanism to toughen the material. Even though toughness values are sporadically characterized in the thiol-ene photopolymerization literature and data is often incomplete, the toughest nonurethane rubbery thiol—ene networks in the literature have values of $\approx 10-50$ MJ m⁻³, $^{47,64-66}$ thus being comparable to the materials presented here. Furthermore, these materials are tougher and more extensible than the existing examples of 3D printed materials that have been degraded and repolymerized using DCB exchange⁴¹⁻⁴⁴ (see Table S9).

2.2. Degradation and Repolymerization. Unlike traditional photopolymer networks, the inclusion of thioester units within the network is useful as a reactive handle for backbone scission. Full degelation of the network occurs in the presence of a >2× molar excess of thiols (per Flory-Stockmayer statistics for step-growth networks⁶⁷) and nucleophilic or basic catalysts due to exchange reactions between thiols and thioesters. 52,68 To extend this concept to semicrystalline networks, tough polymerized networks were immersed in acetone containing an 8× molar excess of PETMP with respect to thioester units and 1 mol equiv of triethylamine (TEA). The 250 μ m micron thick film was observed to dissolve fully over the course of several hours as thiol-thioester exchange reactions degraded the network into soluble oligomers and in accordance with previously developed kinetic models.^{68,69} Subsequent solvent removal yielded a low-viscosity melt, suggesting full degelation (Figure 2A). Size-exclusion chromatography (SEC) confirms that network degradation produces low-molecular-weight oligomers of $M_{\rm N} \approx 800-2700~{\rm g~mol}^{-1}$ (Figure 2B). A large portion of PETMP is also found to persist due to the large excess of this thiol used. Even though full degelation is possible with more modest equivalents of PETMP (Figure S2), these conditions were selected for further study because they produce the lowest-molecularweight and -viscosity oligomers, a key feature needed for vat photopolymerization as discussed later.

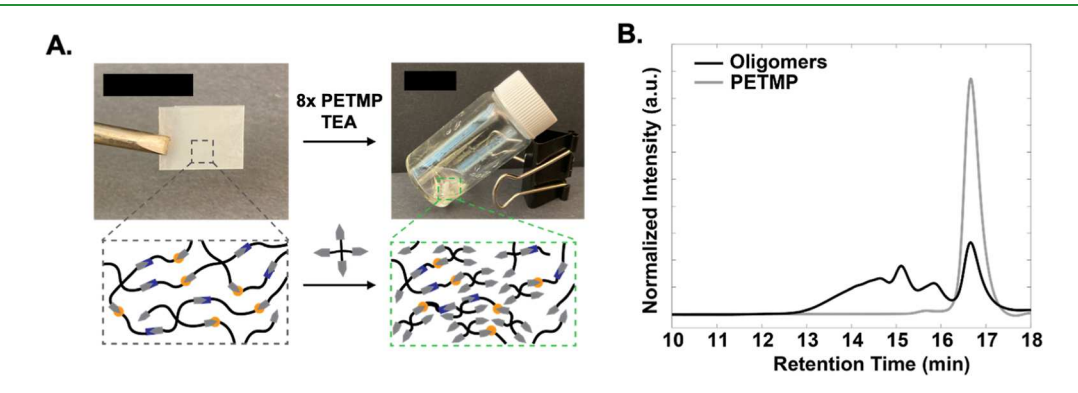


Figure 2. (A) Semicrystalline polymerized networks (left) are observed to degrade into oligomers (left) in the presence of a large excess of tetrafunctional thiol as it adds into the network and pushes them below the gel point (bottom). (B) SEC shows that the networks are degraded into low-molecular-weight oligomers.

Because thiol-thioester exchange preserves the chemical functionality of the native monomers within the oligomeric products (i.e., thiols), these oligomeric products can immediately be repolymerized into new networks. This capability is distinct from other methods such as catalysis⁷⁰ and photodegradation⁷¹ that are often used to fragment polymer backbones, where the collected products cannot be easily incorporated into new materials and various species potentially persist as pollutants, thus exacerbating environmental harm.⁷² While our group has previously shown that A2-B4 step-growth networks could be degraded via thiolthioester exchange and repolymerized with minimal change of crosslink density or mechanical properties, 52 the effects of chain extenders, off-stoichiometric compositions, crystallinity, and morphology were not probed. As such, repolymerizing networks that retain the crystallinity and toughness of the original composition represent a potentially significant advance. Reclaimed oligomers were polymerized with fresh TEDA and DDT, with the excess PETMP persisting from degradation used as the crosslinker, with the molar ratios selected to match the original tough network formulation (Table S5). As shown in Figure 3A, the recycled network (dark blue trace) showed nearly identical thermomechanical properties and crosslink density to the original network (light blue trace). This is corroborated by DSC (Figure 3B), where $\Delta H_{\text{initial}}$ and $\Delta H_{\text{repolymerized}}$ are 45 and 50 J s⁻¹, respectively, suggesting a nearly identical extent and nature of crystallization. These data collectively provide evidence of the

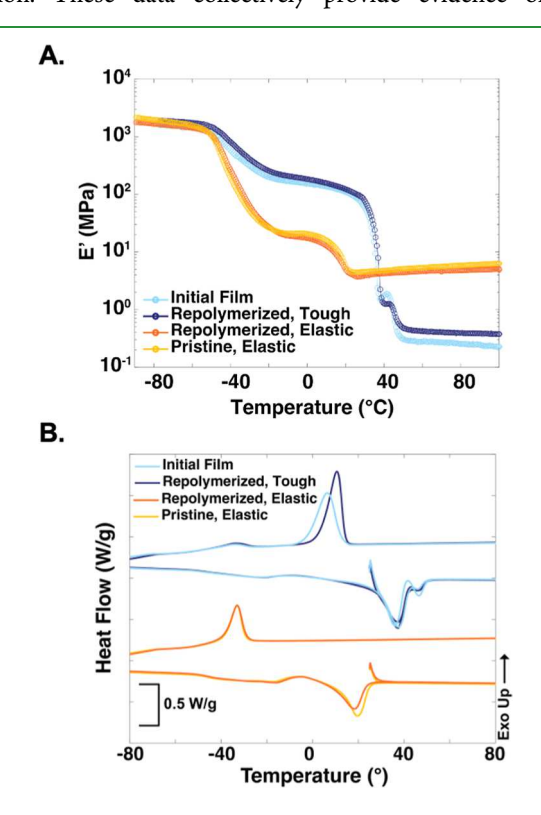


Figure 3. (A) DMA temperature sweeps of different film compositions. Oligomers isolated from degraded tough films (light blue) were repolymerized into new compositions including tough (dark blue) and elastic (orange) networks, with thermomechanical properties that match the pristine films (light blue and yellow). (B) DSC traces show that tough films are crystalline at room temperature, while crystallinity is suppressed in elastic films and that this is consistent before and after recycling/reuse.

preserved network structure across degradation and repolymerization as crystallinity is known to be particularly sensitive to even small changes in network architecture and crosslink density. The persistence of performance following recycling is attributed to the regular network structure achieved through thiol—ene polymerization due to incorporation of structurally regular oligomers. Significantly, the reclaimed network retains Young's modulus of the initial networks and shows only a slight decrease in toughness (20 vs 17 MJ m⁻³) and elongation to break (220 vs 200%), as shown for a representative sample in Figure 4 (blue traces). Finally, the photopolymerization and crystallization kinetics are also largely preserved across recycling (Figure S3).

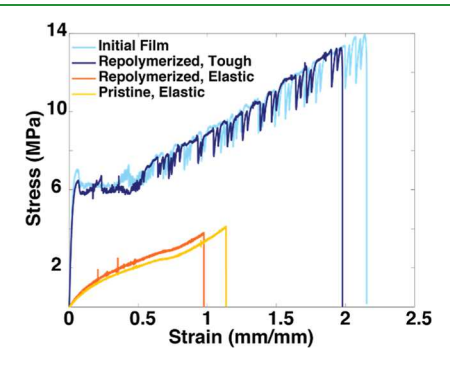


Figure 4. Tensile tests of dogbones made from the composition in Figure 3 show that the conservation of thermomechanical properties results in nearly identical mechanical properties across recycling cycles.

Beyond the synthesis of materials with comparable performance upon recycling, a benefit of chemical degradation over mechanical reprocessing-based approaches to dynamic networks is the ability to use reclaimed oligomers to produce materials with altered, targeted, and desired properties. To demonstrate this approach, the reclaimed oligomers from tough networks were repolymerized into soft and stretchable elastomers using compositions that were previously identified (see Table S6). Specifically, the performance of a pristine network with a composition of 1:1 allyl ether/thiol with 15:85 PETMP/DDT was targeted (herein referred to as the "elastic" composition), which shows higher crosslink density (Figure 3A), suppressed crystallization ($T_{\rm m} \approx 19.5$ °C) (Figure 3B), low modulus (8.6 \pm 0.2 MPa), and modest extensibility (88 \pm 36% strain at break) (Figure 4, yellow curves). Additionally, compared to materials with significant crystallinity at room temperature that plastically deform upon loading, these elastomers nearly fully recover to their initial dimension following deformation (Figure S4). Oligomers from the tough material were successfully repolymerized with TEDA and DDT to yield elastic networks with mechanical properties (Figure 4, orange curves) and photopolymerization kinetics (Figure S5) comparable to the pristine elastic material. These results demonstrate that isolated degradation products can be effectively incorporated with other components to form a variety of materials.

2.3. 3D Printing of Recyclable Resins. To extend this chemistry from bulk polymerized thin films to SLA-based additive manufacturing, resin formulations were screened to optimize printing conditions. Specifically, resins were prepared with 1 wt % TPO and 0.06 wt % pyrogallol as a light absorber. Optimized performance (i.e., limited overcuring and maximum statements).

mized resolution) was observed for 40 s exposure times with 50 μ m layer thickness on a commercially available SLA printer with a 405 nm LED panel ($I \approx 4$ mW cm⁻²). All samples were postcured under flood illumination (405 nm, $I \approx 30$ mW cm⁻²). As a proof-of-concept, the University of Colorado Boulder mascot Ralphie the Buffalo was printed from the tough resin described above to yield a semicrystalline figurine (Figure 5A). Significantly, printed materials are found to

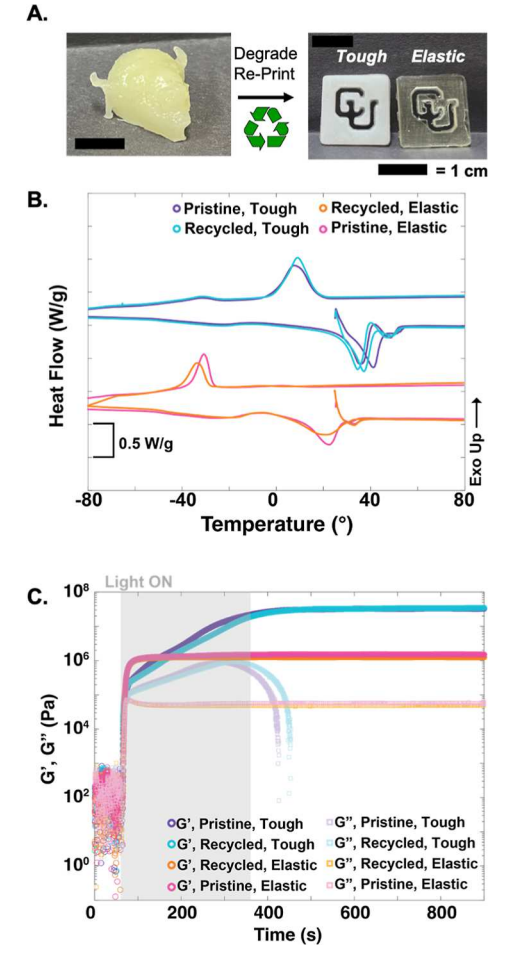


Figure 5. (A) Ralphie the Buffalo, the CU mascot, printed from the tough resin was degraded and used to print new recycled parts (CU Boulder logo, left) that have the same crystalline properties or are elastic and largely amorphous. (B) DSC curves show that thermal transitions and energy release upon crystallizing or melting are conserved in printed parts. (C) Photorheology of printing resins reveals that tough resins start to crystallize as they are polymerized, as shown by the continuous increase in G' over the first 400 s. No crystallization is seen at room temperature for elastic resins, and photopolymerization kinetics are conserved for recycled resins.

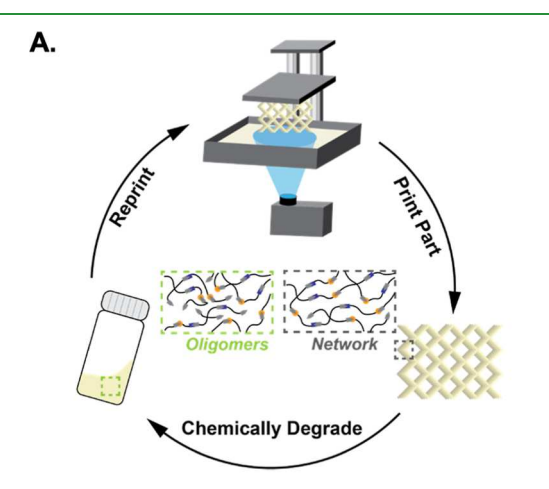
conserve the crystallinity found in bulk films, as evidenced by similar melting enthalpies of 45 and 50. J $\rm g^{-1}$, respectively (Figure 5B). Unlike bulk photopolymerized films, materials printed from the tough resin show a distinct shift in the melting point upon initial heating (blue/purple curves starting at 25 °C) and the second cool and heat cycle (blue/purple curves that span the full temperature range). This outcome is attributed to the subtle changes in crystallization during photopolymerization as observed by photorheology (Figure 5C), where G' increases more quickly following the crossover of G'/G'' compared to bulk samples (Figure S6A). Real-time

FTIR conducted with polymerization conditions selected to match that of the printing compared to bulk films shows a slight decrease in polymerization rate (Figure S6B,C). However, full functional conversion is still observed, with quantitative allyl ether consumption and a small amount of persisting thiol due to the initial 5% stoichiometric excess. This behavior is attributed to a convolution of factors, most notably the inclusion of pyrogallol which could behave as a nucleating agent to increase the crystallization rate and a decreased light intensity (4 vs 10 mW cm⁻²) that slows the polymerization rate. Together, these phenomena likely result in a different and kinetically dictated crystallization pathway compared to bulk polymerized films, where polymerization is fully complete prior to the onset of crystallization. We hypothesize that the slower polymerization rate combined with additives that could potentially act as nucleating agents results in oligomers that can begin to crystallize before full incorporation into the network, compromising the mechanical properties. Additionally, interfacial effects are established to weaken the mechanical performance of printed parts,75 which is likely further exacerbated here where crystallization can impact interlayer adhesion. This manifests as a dramatic change in material properties, and tensile tests revealed that the toughness of printed parts decreased dramatically compared to that of bulk polymerized films (Figure S7), a phenomenon that has been previously observed in other semicrystalline printing resins. 47,60 However, annealing printed dogbones for 1 h at 100 °C and allowing them to cool facilitate recrystallization that is decoupled from the polymerization process, which significantly increased the toughness (Figure S7A). This provides further evidence that the interplay between photopolymerization and crystallization is likely the cause of the compromised mechanical performance. Studies are currently underway to understand the confluence of photopolymerization and crystallization and how to engineer printing methodologies that prevent a deterioration in mechanical performance.

Like bulk films, printed parts were degraded and reprinted into objects with targeted compositions and mechanical properties. As a demonstration, the buffalo printed using the tough resin was degraded under the same conditions used for bulk films, and the isolated oligomers were incorporated into new resin formulations selected to target either tough or elastic performance (as previously shown). We note that while thicker 3D printed parts are likely degraded through a surface-erosion dominated mechanism, thiol-thioester exchange continues in solution and after sufficient time is anticipated to produce oligomers that match those produced by bulk-degradation processes in thin films. The new resins were printed in the shape of the "CU" logo, and the changes in crystallinity could be visibly observed (Figure 5A), where the recycled tough material appeared opaque due to crystallites that scatter light, while the elastic material appeared more optically clear due to a significant reduction in crystallinity. The crystallization of both pristine and recycled tough constructs is largely preserved following degradation and repolymerization, with a slight change in $T_{\rm m}$ and $\Delta H_{\rm m}$ as measured by the second heat cycle of DSC (Figure 5B, blue and purple curves) from 41.2 °C and 46.9 J g⁻¹ to 37.2 °C and 44.7 J g⁻¹, respectively. Additionally, the photopolymerization and crystallization kinetics are strikingly similar, as shown by photorheology (Figure 5C, blue and purple curves) and real-time FTIR (Figure S8), which reveals gelation as allyl ether and thiol groups are quantitatively consumed. As with the pristine tough materials, the recycled

ones show a reduction in mechanical toughness (Figure S7B), likely due to concurrent photopolymerization and crystallization processes that introduce defects into the material when printing, as evidenced by photorheology. In addition to reclaimed tough materials, degraded oligomers could also be incorporated into elastic prints which showed significantly depressed crystallinity at room temperature (Figure 5B, orange and pink) matching that of both pristine elastic printed parts and bulk elastic films. Photorheology revealed no crystallization upon polymerization (Figure 5C, orange and pink), and FTIR showed full consumption of functional groups (Figure S9). Interestingly, compared to the more crystalline materials, printed pristine or recycled elastic dogbones showed mechanical performance that is comparable to that of bulk films. This provides additional evidence that concurrent crystallization and polymerization in printed parts cause a decrease in mechanical performance and suggest that a full decoupling of these processes in future work will greatly improve the toughness of semicrystalline printed parts.

The chemistry of a given polymer network largely governs the mechanical performance and utility of a printed construct. As a demonstration of the emergent device performance achievable with these materials, a lattice was printed using the tough, semicrystalline formulation (Figure 6A,B). These prints are shown to easily support a 100 g wt or >100× its own



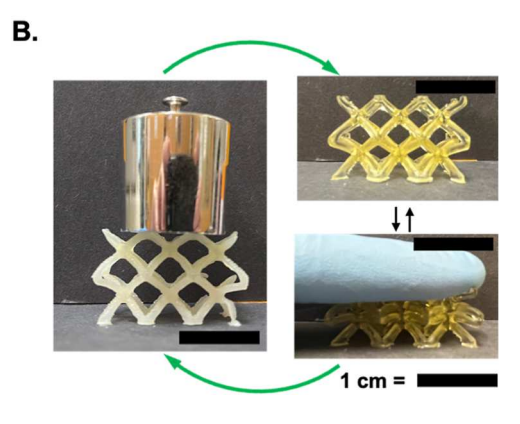


Figure 6. (A) Schematic of printing, degradation, and reprinting processes. (B) Tough resin (left) printed into lattices that support 100 g. Degradation and reprinting with the elastic resin produce a resilient lattice that is easily deformed under a load and springs back. This cycle can then be repeated through another round of degradation and reprinting.

weight due to the high stiffness and toughness of these materials that prevent mechanical failure. However, when degraded with 8× PETMP and repolymerized into the same geometry but with a targeted elastic composition, a soft, deformable lattice is produced (Figure 6B, right). This lattice is easily deformed under an applied load and rebounds to its initial configuration upon removal of the load. Finally, full circularity was realized by degrading the elastic lattice and repolymerizing the resulting oligomers using the correct stoichiometry to target the original tough composition (Figure S10A,B). This approach resulted in a new mechanically strong lattice that matched the load-bearing capabilities of the initial print (Figure S10C). It was noted that these resin compositions are not only comparable with targeted performance metrics of commercial resins⁷⁶ but are also able to be degraded and repolymerized in a way that commercial resins are not. Finally, oligomers were also combined with other functionalities such as acrylates which are often employed in commercial resins, providing the opportunity to modulate existing formulations (Figure S11). Thus, this system opens opportunities to reduce waste while retaining the desired mechanical properties.

2.4. Advanced Capabilities: Resin Modulation, Shape Memory, and Self-Healing. The ability to degrade these mechanically diverse materials into universal thiol-functional chemical building blocks additionally opens opportunities for "single-stream" recycling. One major hurdle to recycling broadly is that polymeric items with different properties are typically assembled using distinct polymer backbones, necessitating the need for manual separation prior to reprocessing due to material incompatibility. Here, the entire resin formulation is simultaneously degraded, and the products combined to produce an array of potential new networks. As a demonstration of this approach, both tough and elastic printed materials were degraded with 8× PETMP and polymerized in different proportions with a triallyl crosslinker at a 1:1 thiol/ allyl ether ratio (Figure 7A, left). Films containing 100% tough oligomers, 100% elastic oligomers, and 50/50 combination of each were polymerized, and the thermomechanical properties were probed using DMA (Figure 7A, right). The temperature at peak and the width of tan δ (Figure 7A, inset) in addition to the final plateau modulus of G' were nearly perfectly matched, suggesting that the network structure is identical for all compositions. Monomer conversion and polymerization kinetics were also comparable for all formulations (Figure S12). Furthermore, these compositions were printed into new objects, as demonstrated by the formation of a bighorn sheep, the state animal of Colorado (Figure 7B). Thus, in principle, parts printed from these resins can be degraded in one-pot processes without separation and printed into new materials, significantly streamlining the recycling process.

While chemical recyclability facilitates full end-of-life control, an additional goal of sustainability is the incorporation of mechanisms for postprinting modification to control material performance over the lifetime of the object. The simultaneous inclusion of both dynamic chemistry and crystallinity facilitates the ability to augment or repair a structure as needed, thus presenting the opportunity to extend the useful lifetime of a printed part. Specifically, melting and recrystallization facilitate shape change of a printed object (see Figure S13 for complete shape memory analysis). As a demonstration of this, an octopus was printed from the tough resin (Figure 8, top). Upon heating to 100 °C, the

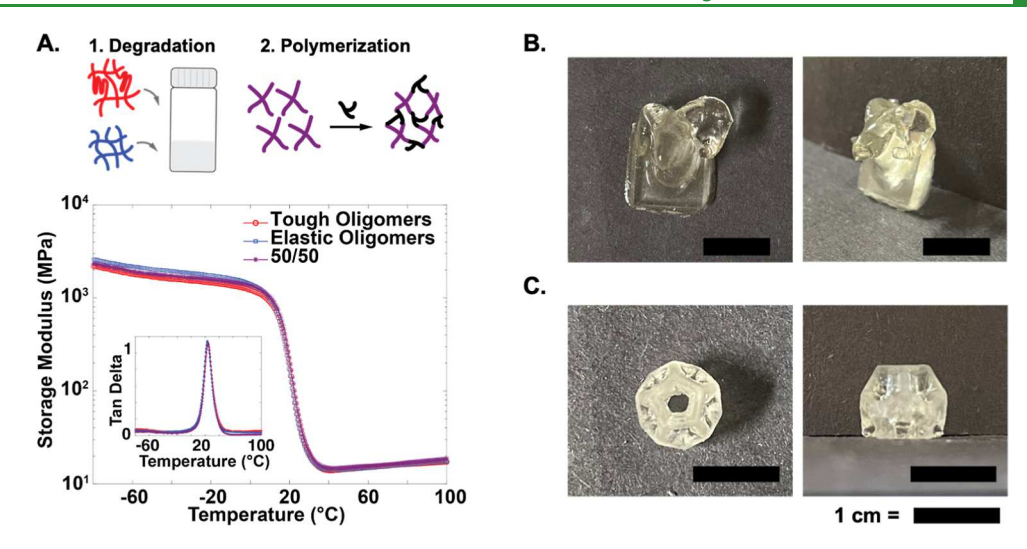


Figure 7. (A) Schematic of degradation and polymerization (top) of both tough and elastic materials for "single-stream" recycling. When varying feedstocks of oligomers are polymerized with a trifunctional allyl ether, networks with nearly identical thermomechanical properties are produced (bottom). Resins containing a 50/50 mixture of oligomers produced from tough or elastic components were printed into objects such as a (B) bighorn sheep or (C) a tetrahedron.

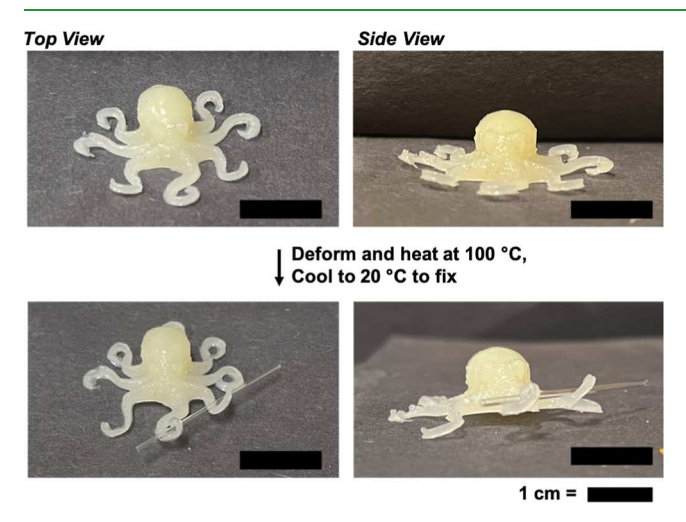


Figure 8. Crystallinity of the tough resins facilitates shape memory. As a demonstration, a printed octopus can be heated above the melting point, its legs raised to hold a pipette, and cooled to lock this new conformation in as the object recrystallizes.

object melted but retained its shape due to the incorporated crosslinks and was subsequently manipulated into a new shape that is "locked in" upon cooling and reformation of crystallites. For example, the arms of the octopus can be raised to hold a thin glass capillary under heating and fixed in this configuration upon cooling (Figure 8, bottom). Beyond simple metastable configurations facilitated by crystallization, the incorporated dynamic chemistry was exploited for permanent and constructive modulation. As shown in Figure 9, when a printed cactus is severed from the pot it is attached to, it can be "replanted" by activating dynamic chemistry at the interface between the cactus and the plant to permanently repair the object. Self-healing is catalyzed by placing a drop of TEA between the cactus and pot, manually fixing them together, and heating the material for 2 h at 100 °C (Figure 9). The residual thiols within the network facilitate exchange with thioester groups in response to the TEA (Figure S14), allowing covalent bonds to form between the two parts and coalesce the network of each part together. Finally, representative tests on thin films

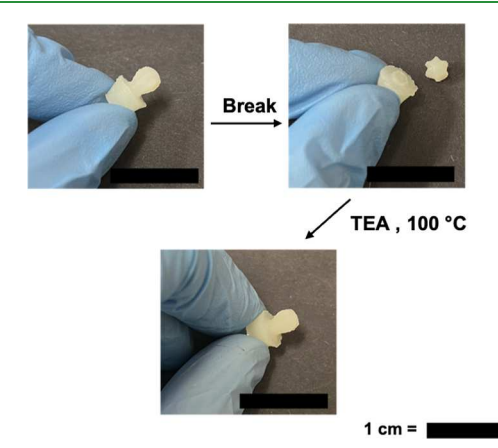


Figure 9. Interfacial thiol—thioester exchange reactions can facilitate self-healing. As a demonstration, a cactus in a pot was printed and cut in half (top). Application of TEA at the interface between the severed parts facilitates bond exchange and healing of the object in the presence of heat to reproduce the initial object.

show that healed samples regain their initial mechanical performance (Figure S15).

3. CONCLUSIONS

Advancing vat photopolymerization-based additive manufacturing relies on developing new strategies to produce materials using light with desired mechanical performance that are also amenable to life cycle control. The chemical platform developed here of incorporating thioester functionality within semicrystalline networks was shown to produce tough, thermoplastic-like crosslinked materials. These materials were shown to be amenable to degradation into functional oligomers that could be reincorporated into recycled tough materials or elastic materials depending on the stoichiometry used. Significantly, these materials are compatible with SLA 3D printing, and constructs were printed and recycled into materials with targeted mechanical performance and capabilities. Finally, the combination of crystallization and dynamic chemistry also facilitates transformation of printed parts via shape memory and self-healing, providing routes to modulate

printed parts over intermediate timescales and reduce singleuse components. In the future, careful engineering of photopolymerization kinetics and crystalline self-assembly will yield printed parts with even greater toughness and mechanical versatility. Additionally, thioester groups can likely be incorporated into other structured polymer systems including those containing nanoscale ordering or mesophases, thus providing new opportunities for both controlling polymer assembly on small scales, macroscopic performance, and global recyclability simultaneously.

4. EXPERIMENTAL SECTION

- **4.1. Materials.** All materials were purchased from common suppliers (Tokyo Chemical Industries, MilliporeSigma, Fisher Scientific, and Alpha Aesar) and used as received without further purification. The reactants and monomers used include succinic anhydride, 3-mercaptopropionic acid, *p*-toluenesulfonic acid monohydrate, allyl alcohol, DDT, PETMP, TPO, pyrogallol, 4-dimethylaminopyridine (DMAP), pyridine, TEA, and sodium sulfate (Na₂SO₄). Common solvents used include acetonitrile (MeCN), ethyl acetate, hexanes, and dichloromethane.
- **4.2.** Synthesis of the Thioester Diallyl Monomer. The thioester diallyl monomer used in these materials was synthesized in two steps according to a previous report. So In the first step, 50.0 g (500 mmol, 1 equiv) of succinic anhydride was combined in a 1 L round-bottom flask with 50 mL of pyridine and 450 mL of acetonitrile. The sample was stirred using a magnetic stir bar until the solution was homogeneous. Subsequently, 53.0 g (500 mmol, 1.0 equiv) of 3-mercaptopropionic acid was added, followed by 3.05 g (25.0 mmol, 0.05 equiv) of DMAP. The solution was stirred overnight at room temperature. Following the completion of the reaction, the solvent was removed under rotary evaporation, and the viscous residue was dissolved in \approx 500 mL of ethyl acetate. The crude product was washed with 1 N HCl and back extracted with additional EtOAc, and the organics were dried with Na₂SO₄. A white powder was isolated following the removal of EtOAc.

In the second step, 40.0 g (194 mmol, 1.0 equiv) of the isolated product, 55.2 g (388 mmol, 2.0 equiv) of Na_2SO_4 , and 3.69 g (19.4 mmol, 0.1 equiv) of p-toluenesulfonic acid monohydrate (TsOH- H_2O) were added to a 1 L round-bottom flask affixed with a football-shaped stir bar. These solids were diluted with 400 mL (0.5 M) of toluene and stirred to create an opaque suspension. Finally, 52.8 mL (776 mmol, 4.0 equiv) of allyl alcohol was added, the round-bottom flask was fixed with a reflux condenser, and the whole reaction was heated to 85 °C under rapid stirring. After 12 h of reaction time, the solution was cooled to room temperature and filtered to remove the solids, and the crude product was isolated as a slightly viscous oil by rotary evaporation. The crude product was subjected to column chromatography (10% \rightarrow 30% EtOAc/hexanes) and isolated as a clear oil

- **4.3. General Photopolymerization Procedure.** To polymerize bulk films, all reactants (i.e., TEDA, DDT, PETMP, and/or degraded oligomers) were combined in a scintillation vial. The low-viscosity monomer solution was mixed thoroughly using a vortex mixer until it became homogeneous. Then, TPO (1 wt %) was added to the vial, and the reaction mixture was heated gently using a heat gun until all TPO was dissolved. The resin was pipetted onto a clean glass slide treated with Rain-X, sandwiched between another Rain-X-coated glass slide with 250 μ m plastic spacers, and exposed to a 405 nm LED (\approx 10 mW cm $^{-2}$) for 5 min. Following polymerization, films were harvested using a razor blade.
- **4.4. Degradation.** In a representative procedure, planar films or printed disks of prescribed weight were added to a clean 50 mL round-bottom flask equipped with a stir bar. Then, PETMP (8.0 equiv of thiol functional groups with respect to thioester functional groups in the networks) was added to the flask. This was diluted with acetone (1 equiv by weight to PETMP) and stirred vigorously until all PETMP was dissolved. Finally, TEA (1 equiv with respect to

- PETMP) was added, and the reaction mixture was stirred for 12 h. After this, a homogeneous solution was formed, and acetone was removed under rotary evaporation. Finally, TEA was removed under high vacuum at 80 $^{\circ}\text{C}$ for several hours until all TEA was gone as monitored by TLC and ^{1}H NMR. The oligomers were stored in a freezer until use.
- 4.5. 3D Printing. Printed constructs were made using a commercially available SLA printer (PRUSA SL1, PRUSA Research) with a measured light intensity of ≈4 mW cm⁻² at 405 nm. Resin formulations were prepared in the same way as that for bulk films but with 0.5 wt % TPO and 0.06 wt % pyrogallol. Resin formulations were prepared in 10 g batches, stirred at 60 °C for several minutes until all solids were dissolved, and poured into the printer's resin bath. Print designs were adapted from open-source CAD files (MakerBot Thingiverse) and sliced into projection patterns (PrusaSlicer). Constructs were printed using layers of a thickness of 100 μ m and 40 s exposure times per layer. Following printing, the printing platform was removed from the printed part, excess resin was carefully removed using a gentle stream of compressed air, the bulk object was cured under flood illuminations (405 nm, 30 mW cm⁻²) to encourage full polymerization, and finally, the object was removed from the printing platform using a razor blade.
- **4.6. Dynamic Mechanical Analysis.** Temperature sweeps were performed on an RSA-G2 DMA (TA Instruments) using 0.3% strain, a frequency of 1 Hz, and a heating rate of 3 °C min⁻¹. Samples of approximately 10 mm × 5 cm × 0.25 cm (length × width × thickness) were loaded into the clamps, cooled to -90 °C, and held isothermal for 10 min prior to the start of the test to ensure complete crystallization.
- **4.7. Photorheology.** In situ photopolymerization and crystallization kinetics were probed using an ARES-G2 rheometer (TA Instruments). A drop of the resin sample was placed on a Peltier plate held at 25 °C, and the transducer fixed with a 10 mm glass plate was lowered to a gap size of 100 μ m. The samples were irradiated through the glass plate for 5 min, while the sample was subject to 1% strain at 1 Hz. Following irradiation, the sample was monitored for 60 min to monitor modulus evolution over time as the sample crystallized.
- **4.8. FTIR Spectroscopy.** Polymerization kinetics were measured in situ using an FTIR spectrometer (Nicolet 6700, Thermo Scientific) with an MCT/A detector with a transmission accessory. A drop of resin was placed between two KBr plates and irradiated from above. Functional group conversion was monitored over time with a scan speed of 2 scans/second for thiol (2630–2483 cm⁻¹) and allyl ether groups (1659–1635 cm⁻¹) by integrating peak area data using OMNIC software (Thermo Scientific).
- **4.9. Differential Scanning Calorimetry.** Crystallinity and thermal transitions were probed using a Discovery DSC 2500 (TA Instruments). For each measurement, 5-10 mg of the sample cut was sealed into a DSC pan and subject to heating and cooling rates of 10 °C s⁻¹.
- **4.10. Self-Healing Test.** A 3D print of a cactus in a pot (Thingiverse) was prepared as described above. A sharp razor blade was used to sever the object into two pieces. A small drop of TEA was placed on one severed surfaced, and the detached part was placed on top, bringing together the two freshly cut surfaces. The whole construct was placed in a 100 °C oven for 2 h to facilitate dynamic exchange and self-healing. To quantify self-healing, samples of approximately 6 mm × 10 cm × 0.25 cm (length × width × thickness) were cut in half and heated to 100 °C. A drop of TEA was added, and the films were overlapped by approximately 5 mm. Samples were placed between Rain-X-treated glass slides, held under pressure with binder clips, and heated to 100 °C for 2 h. Following this treatment, the samples were approximately 0.2 cm in thickness and there was not a distinct difference in thickness where overlap had occurred. Tensile testing was then performed to assess the mechanical properties.
- **4.11. Shape-Memory Test.** A 3D print of an octopus (Thingiverse) was prepared as described previously. To distort the construct, the print was heated to 100 °C in an oven for several minutes to ensure uniform melting. When fully melted, the print was

removed from the oven, fixed into a new configuration, and held in this geometry for 2 h, while the object cooled and recrystallized. Quantification of shape memory recovery was performed on an RSA-G2 DMA (TA Instruments). Samples of approximately 6 mm \times 10 cm \times 0.25 cm (length \times width \times thickness) were loaded into the clamps and heated to 25 °C while equilibrating at 0 load force. Samples were then heated to 100 °C at a rate of 13 °C/min under constant force and held for 5 min. Strain was then set to 100% relative to the current length, and the samples were cooled to 25 °C at 13 °C/min at the set strain. The temperature was held constant for 30 min to allow for crystallization, after which the strain was allowed to adjust such that minimal force remained over a 5 min period. Samples were then heated to 100 °C under constant force. Recovery was assessed between the initial and final length at 100 °C.

ASSOCIATED CONTENT

Supporting Information

The Supporting Information is available free of charge at https://pubs.acs.org/doi/10.1021/acsami.2c22081.

Additional experimental details and the corresponding data (PDF)

AUTHOR INFORMATION

Corresponding Author

Christopher N. Bowman — Department of Chemical and Biological Engineering, University of Colorado Boulder, Boulder, Colorado 80309, United States; Materials Science and Engineering Program, University of Colorado Boulder, Boulder, Colorado 80309, United States; orcid.org/0000-0001-8458-7723; Email: christopher.bowman@colorado.edu

Authors

Alexa S. Kuenstler — Department of Chemical and Biological Engineering, University of Colorado Boulder, Boulder, Colorado 80309, United States; Present Address: Department of Chemical and Biomolecular Engineering, University of Illinois at Urbana-Champaign, Urbana, Illinois 61801, United States; orcid.org/0000-0003-0432-2173

Juan J. Hernandez — Department of Chemical and Biological Engineering, University of Colorado Boulder, Boulder, Colorado 80309, United States; orcid.org/0000-0003-0040-0904

Marianela Trujillo-Lemon — Department of Chemical and Biological Engineering, University of Colorado Boulder, Boulder, Colorado 80309, United States

Alexander Osterbaan — Department of Chemical and Biological Engineering, University of Colorado Boulder, Boulder, Colorado 80309, United States

Complete contact information is available at: https://pubs.acs.org/10.1021/acsami.2c22081

Author Contributions

The manuscript was written through contributions of all authors. All authors have given approval to the final version of the manuscript.

Notes

The authors declare no competing financial interest.

ACKNOWLEDGMENTS

The authors thank Timothy J. White for use of DSC and Kyle Schlafmann for help with the experimental setup. C.N.B.

acknowledges support from the NSF (CHE 1808484). A.S.K. acknowledges support from an Arnold O. Beckman Post-Doctoral Fellowship.

REFERENCES

- (1) Truby, R. L.; Lewis, J. A. Printing Soft Matter in Three Dimensions. *Nature* **2016**, *540*, 371–378.
- (2) Zhou, L.-Y.; Fu, J.; He, Y. A Review of 3D Printing Technologies for Soft Polymer Materials. *Adv. Funct. Mater.* **2020**, *30*, 2000187.
- (3) Appuhamillage, G. A.; Chartrain, N.; Meenakshisundaram, V.; Feller, K. D.; Williams, C. B.; Long, T. E. 110th Anniversary: Vat Photopolymerization-Based Additive Manufacturing: Current Trends and Future Directions in Materials Design. *Ind. Eng. Chem. Res.* **2019**, *58*, 15109–15118.
- (4) Boydston, A. J.; Cui, J.; Lee, C.-U.; Lynde, B. E.; Schilling, C. A. 100th Anniversary of Macromolecular Science Viewpoint: Integrating Chemistry and Engineering to Enable Additive Manufacturing with High-Performance Polymers. *ACS Macro Lett.* **2020**, *9*, 1119–1129.
- (5) Guo, S.-Z.; Gosselin, F.; Guerin, N.; Lanouette, A.-M.; Heuzey, M.-C.; Therriault, D. Solvent-Cast Three-Dimensional Printing of Multifunctional Microsystems. *Small* **2013**, *9*, 4118–4122.
- (6) Wang, P.; Zou, B.; Xiao, H.; Ding, S.; Huang, C. Effects of Printing Parameters of Fused Deposition Modeling on Mechanical Properties, Surface Quality, and Microstructure of PEEK. *J. Mater. Process. Technol.* **2019**, 271, 62–74.
- (7) Fitzharris, E. R.; Watt, I.; Rosen, D. W.; Shofner, M. L. Interlayer Bonding Improvement of Material Extrusion Parts with Polyphenylene Sulfide Using the Taguchi Method. *Addit. Manuf.* **2018**, *24*, 287–297.
- (8) Schirmeister, C. G.; Hees, T.; Licht, E. H.; Mülhaupt, R. 3D Printing of High Density Polyethylene by Fused Filament Fabrication. *Addit. Manuf.* **2019**, *28*, 152–159.
- (9) Zhu, J.; Hu, Y.; Tang, Y.; Wang, B. Effects of Styrene–Acrylonitrile Contents on the Properties of ABS/SAN Blends for Fused Deposition Modeling. J. Appl. Polym. Sci. 2017, 134, 44477.
- (10) Highley, C. B.; Rodell, C. B.; Burdick, J. A. Direct 3D Printing of Shear-Thinning Hydrogels into Self-Healing Hydrogels. *Adv. Mater.* **2015**, *27*, 5075–5079.
- (11) Sydney Gladman, A.; Matsumoto, E. A.; Nuzzo, R. G.; Mahadevan, L.; Lewis, J. A. Biomimetic 4D Printing. *Nat. Mater.* **2016**, *15*, 413–418.
- (12) Liu, W.; Heinrich, M. A.; Zhou, Y.; Akpek, A.; Hu, N.; Liu, X.; Guan, X.; Zhong, Z.; Jin, X.; Khademhosseini, A.; Zhang, Y. S. Extrusion Bioprinting of Shear-Thinning Gelatin Methacryloyl Bioinks. *Adv. Healthcare Mater.* **2017**, *6*, 1601451.
- (13) Jang, S.; Boddorff, A.; Jang, D. J.; Lloyd, J.; Wagner, K.; Thadhani, N.; Brettmann, B. Effect of Material Extrusion Process Parameters on Filament Geometry and Inter-filament Voids in As-Fabricated High Solids Loaded Polymer Composites. *Addit. Manuf.* **2021**, *47*, 102313.
- (14) Ning, F.; Cong, W.; Hu, Y.; Wang, H. Additive Manufacturing of Carbon Fiber-Reinforced Plastic Composites Using Fused Deposition Modeling: Effects of Process Parameters on Tensile Properties. J. Compos. Mater. 2017, 51, 451–462.
- (15) Çantı, E.; Aydın, M. Effects of Micro Particle Reinforcement on Mechanical Properties of 3D Printed Parts. *Rapid Prototyp. J.* **2018**, 24, 171–176.
- (16) McBride, M. K.; Worrell, B. T.; Brown, T.; Cox, L. M.; Sowan, N.; Wang, C.; Podgorski, M.; Martinez, A. M.; Bowman, C. N. Enabling Applications of Covalent Adaptable Networks. *Annu. Rev. Chem. Biomol. Eng.* **2019**, *10*, 175–198.
- (17) Scheutz, G. M.; Lessard, J. J.; Sims, M. B.; Sumerlin, B. S. Adaptable Crosslinks in Polymeric Materials: Resolving the Intersection of Thermoplastics and Thermosets. *J. Am. Chem. Soc.* **2019**, *141*, 16181–16196.
- (18) Winne, J. M.; Leibler, L.; Du Prez, F. E. Dynamic Covalent Chemistry in Polymer Networks: A Mechanistic Perspective. *Polym. Chem.* **2019**, *10*, 6091–6108.

- (19) Montarnal, D.; Capelot, M.; Tournilhac, F.; Leibler, L. Silicalike Malleable Materials from Permanent Organic Networks. *Science* **2011**, 334, 965–968.
- (20) Ishibashi, J. S. A.; Kalow, J. A. Vitrimeric Silicone Elastomers Enabled by Dynamic Meldrum's Acid-Derived Cross-Links. *ACS Macro Lett.* **2018**, *7*, 482–486.
- (21) Lessard, J. J.; Garcia, L. F.; Easterling, C. P.; Sims, M. B.; Bentz, K. C.; Arencibia, S.; Savin, D. A.; Sumerlin, B. S. Catalyst-Free Vitrimers from Vinyl Polymers. *Macromolecules* **2019**, *52*, 2105–2111.
- (22) Zhang, B.; Digby, Z. A.; Flum, J. A.; Chakma, P.; Saul, J. M.; Sparks, J. L.; Konkolewicz, D. Dynamic Thiol—Michael Chemistry for Thermoresponsive Rehealable and Malleable Networks. *Macromolecules* **2016**, *49*, 6871–6878.
- (23) Porath, L.; Huang, J.; Ramlawi, N.; Derkaloustian, M.; Ewoldt, R. H.; Evans, C. M. Relaxation of Vitrimers with Kinetically Distinct Mixed Dynamic Bonds. *Macromolecules* **2022**, *55*, 4450–4458.
- (24) Lu, Y. X.; Guan, Z. Olefin Metathesis for Effective Polymer Healing via Dynamic Exchange of Strong Carbon-Carbon Double Bonds. J. Am. Chem. Soc. 2012, 134, 14226–14231.
- (25) Capelot, M.; Montarnal, D.; Tournilhac, F.; Leibler, L. Metal-Catalyzed Transesterification for Healing and Assembling of Thermosets. J. Am. Chem. Soc. 2012, 134, 7664–7667.
- (26) Denissen, W.; Droesbeke, M.; Nicolaÿ, R.; Leibler, L.; Winne, J. M.; Du Prez, F. E. Chemical Control of the Viscoelastic Properties of Vinylogous Urethane Vitrimers. *Nat. Commun.* **2017**, *8*, 14857.
- (27) Self, J. L.; Dolinski, N. D.; Zayas, M. S.; Read de Alaniz, J.; Bates, C. M. Brønsted-Acid-Catalyzed Exchange in Polyester Dynamic Covalent Networks. *ACS Macro Lett.* **2018**, *7*, 817–821.
- (28) Fortman, D. J.; Sheppard, D. T.; Dichtel, W. R. Reprocessing Cross-Linked Polyurethanes by Catalyzing Carbamate Exchange. *Macromolecules* **2019**, *52*, 6330–6335.
- (29) Michal, B. T.; Jaye, C. A.; Spencer, E. J.; Rowan, S. J. Inherently Photohealable and Thermal Shape-Memory Polydisulfide Networks. *ACS Macro Lett.* **2013**, *2*, 694–699.
- (30) Accardo, J. V.; McClure, E. R.; Mosquera, M. A.; Kalow, J. A. Using Visible Light to Tune Boronic Acid—Ester Equilibria. *J. Am. Chem. Soc.* **2020**, *142*, 19969—19979.
- (31) Scott, T. F.; Schneider, A. D.; Cook, W. D.; Bowman, C. N. Photoinduced Plasticity in Cross-Linked Polymers. *Science* **2005**, *308*, 1615–1617
- (32) Li, L.; Chen, X.; Jin, K.; Torkelson, J. M. Vitrimers Designed Both To Strongly Suppress Creep and To Recover Original Cross-Link Density after Reprocessing: Quantitative Theory and Experiments. *Macromolecules* **2018**, *51*, 5537–5546.
- (33) Meng, F.; Saed, M. O.; Terentjev, E. M. Elasticity and Relaxation in Full and Partial Vitrimer Networks. *Macromolecules* **2019**, *52*, 7423–7429.
- (34) Dahlke, J.; Zechel, S.; Hager, M. D.; Schubert, U. S. How to Design a Self-Healing Polymer: General Concepts of Dynamic Covalent Bonds and Their Application for Intrinsic Healable Materials. *Adv. Mater. Interfaces* **2018**, *5*, 1800051.
- (35) Melchor Bañales, A. J.; Larsen, M. B. Thermal Guanidine Metathesis for Covalent Adaptable Networks. *ACS Macro Lett.* **2020**, 9, 937–943.
- (36) Kuang, X.; Zhou, Y.; Shi, Q.; Wang, T.; Qi, H. J. Recycling of Epoxy Thermoset and Composites via Good Solvent Assisted and Small Molecules Participated Exchange Reactions. ACS Sustainable Chem. Eng. 2018, 6, 9189–9197.
- (37) Hamachi, L. S.; Rau, D. A.; Arrington, C. B.; Sheppard, D. T.; Fortman, D. J.; Long, T. E.; Williams, C. B.; Dichtel, W. R. Dissociative Carbamate Exchange Anneals 3D Printed Acrylates. *ACS Appl. Mater. Interfaces* **2021**, *13*, 38680–38687.
- (38) Podgórski, M.; Huang, S.; Bowman, C. N. Additive Manufacture of Dynamic Thiol—Ene Networks Incorporating Anhydride-Derived Reversible Thioester Links. ACS Appl. Mater. Interfaces 2021, 13, 12789—12796.
- (39) Robinson, L. L.; Self, J. L.; Fusi, A. D.; Bates, M. W.; Read de Alaniz, J.; Hawker, C. J.; Bates, C. M.; Sample, C. S. Chemical and

- Mechanical Tunability of 3D-Printed Dynamic Covalent Networks Based on Boronate Esters. ACS Macro Lett. 2021, 10, 857–863.
- (40) Rossegger, E.; Höller, R.; Reisinger, D.; Strasser, J.; Fleisch, M.; Griesser, T.; Schlögl, S. Digital Light Processing 3D Printing with Thiol—Acrylate Vitrimers. *Polym. Chem.* **2021**, *12*, 639–644.
- (41) Zhang, B.; Kowsari, K.; Serjouei, A.; Dunn, M. L.; Ge, Q. Reprocessable Thermosets for Sustainable Three-Dimensional Printing. *Nat. Commun.* **2018**, *9*, 1831.
- (42) Shi, Q.; Yu, K.; Kuang, X.; Mu, X.; Dunn, C. K.; Dunn, M. L.; Wang, T.; Jerry Qi, H. Recyclable 3D Printing of Vitrimer Epoxy. *Mater. Horiz.* **2017**, *4*, 598–607.
- (43) Chen, Z.; Yang, M.; Ji, M.; Kuang, X.; Qi, H. J.; Wang, T. Recyclable Thermosetting Polymers for Digital Light Processing 3D Printing. *Mater. Des.* **2021**, *197*, 109189.
- (44) Zhu, G.; Zhang, J.; Huang, J.; Qiu, Y.; Liu, L.; Yu, J.; Liu, C.; Shang, Q.; Hu, Y.; Hu, L.; Zhou, Y. Recyclable and Reprintable Biobased Photopolymers for Digital Light Processing 3D Printing. *Chem. Eng. J.* **2023**, 452, 139401.
- (45) Hoyle, C. E.; Bowman, C. N. Thiol-Ene Click Chemistry. *Angew. Chem., Int. Ed.* **2010**, 49, 1540–1573.
- (46) Hoffmann, A.; Kreuels, K.; Gillner, A. Novel Thiol-Ene Photo Resins for Stereolithography with Enhanced Mechanical and Optical Properties. *Macromol. Mater. Eng.* **2022**, 307, 2100625.
- (47) Sycks, D. G.; Wu, T.; Park, H. S.; Gall, K. Tough, Stable Spiroacetal Thiol-Ene Resin for 3D Printing. *J. Appl. Polym. Sci.* **2018**, 135, 46259.
- (48) Chen, L.; Wu, Q.; Wei, G.; Liu, R.; Li, Z. Highly Stable Thiol—Ene Systems: From Their Structure—Property Relationship to DLP 3D Printing. *J. Mater. Chem. C* **2018**, *6*, 11561—11568.
- (49) Ahn, D.; Stevens, L. M.; Zhou, K.; Page, Z. A. Additives for Ambient 3D Printing with Visible Light. *Adv. Mater.* **2021**, *33*, 2104906.
- (50) Shahzadi, L.; Maya, F.; Breadmore, M. C.; Thickett, S. C. Functional Materials for DLP-SLA 3D Printing Using Thiol—Acrylate Chemistry: Resin Design and Postprint Applications. *ACS Appl. Polym. Mater.* **2022**, *4*, 3896—3907.
- (51) Worrell, B. T.; McBride, M. K.; Lyon, G. B.; Cox, L. M.; Wang, C.; Mavila, S.; Lim, C. H.; Coley, H. M.; Musgrave, C. B.; Ding, Y.; Bowman, C. N. Bistable and Photoswitchable States of Matter. *Nat. Commun.* **2018**, *9*, 2804.
- (52) Wang, C.; Goldman, T. M.; Worrell, B. T.; McBride, M. K.; Alim, M. D.; Bowman, C. N. Recyclable and Repolymerizable Thiol-X Photopolymers. *Mater. Horiz.* **2018**, *5*, 1042–1046.
- (53) Podgórski, M.; Spurgin, N.; Mavila, S.; Bowman, C. N. Mixed Mechanisms of Bond Exchange in Covalent Adaptable Networks: Monitoring the Contribution of Reversible Exchange and Reversible Addition in Thiol-Succinic Anhydride Dynamic Networks. *Polym. Chem.* **2020**, *11*, 5365–5376.
- (54) Soars, S. M.; Bongiardina, N. J.; Fairbanks, B. D.; Podgórski, M.; Bowman, C. N. Spatial and Temporal Control of Photomediated Disulfide—Ene and Thiol—Ene Chemistries for Two-Stage Polymerizations. *Macromolecules* **2022**, *55*, 1811–1821.
- (55) Shin, J.; Matsushima, H.; Chan, J. W.; Hoyle, C. E. Segmented Polythiourethane Elastomers through Sequential Thiol—Ene and Thiol—Isocyanate Reactions. *Macromolecules* **2009**, *42*, 3294—3301.
- (56) McNair, O. D.; Brent, D. P.; Sparks, B. J.; Patton, D. L.; Savin, D. A. Sequential Thiol Click Reactions: Formation of Ternary Thiourethane/Thiol—Ene Networks with Enhanced Thermal and Mechanical Properties. ACS Appl. Mater. Interfaces 2014, 6, 6088—6097.
- (57) Shin, J.; Matsushima, H.; Comer, C. M.; Bowman, C. N.; Hoyle, C. E. Thiol–Isocyanate–Ene Ternary Networks by Sequential and Simultaneous Thiol Click Reactions. *Chem. Mater.* **2010**, 22, 2616–2625.
- (58) Song, H. B.; Baranek, A.; Worrell, B. T.; Cook, W. D.; Bowman, C. N. Photopolymerized Triazole-Based Glassy Polymer Networks with Superior Tensile Toughness. *Adv. Funct. Mater.* **2018**, 28, 1801095.

- (59) Silikas, N.; Watts, D. C. Rheology of Urethane Dimethacrylate and Diluent Formulations. *Dent. Mater.* **1999**, *15*, 257–261.
- (60) Childress, K. K.; Alim, M. D.; Hernandez, J. J.; Stansbury, J. W.; Bowman, C. N. Additive Manufacture of Lightly Crosslinked Semicrystalline Thiol-Enes for Enhanced Mechanical Performance. *Polym. Chem.* **2019**, *11*, 39–46.
- (61) Zhong, M.; Wang, R.; Kawamoto, K.; Olsen, B. D.; Johnson, J. A. Quantifying the Impact of Molecular Defects on Polymer Network Elasticity. *Science* **2016**, 353, 1264–1268.
- (62) Barney, C. W.; Ye, Z.; Sacligil, I.; McLeod, K. R.; Zhang, H.; Tew, G. N.; Riggleman, R. A.; Crosby, A. J. Fracture of Model End-Linked Networks. *Proc. Natl. Acad. Sci. U.S.A.* **2022**, 119, No. e2112389119.
- (63) Séguéla, R. On the Natural Draw Ratio of Semi-Crystalline Polymers: Review of the Mechanical, Physical and Molecular Aspects. *Macromol. Mater. Eng.* **2007**, 292, 235–244.
- (64) Donovan, B. R.; Ballenas, J. E.; Patton, D. L. Thiol—Trifluorovinyl Ether (TFVE) Photopolymerization: An On-Demand Synthetic Route to Semifluorinated Polymer Networks. *Macromolecules* **2016**, *49*, 7667–7675.
- (65) Khalfa, A. L.; Becker, M. L.; Dove, A. P. Stereochemistry-Controlled Mechanical Properties and Degradation in 3D-Printable Photosets. *J. Am. Chem. Soc.* **2021**, *143*, 17510–17516.
- (66) Ding, R.; Du, Y.; Goncalves, B. R.; Francis, F. L.; Reineke, M. T. Sustainable near UV-Curable Acrylates Based on Natural Phenolics for Stereolithography 3D Printing. *Polym. Chem.* **2019**, *10*, 1067–1077
- (67) Odian, G. Principles of Polymerization, 4th ed.; John Wiley & Sons, Inc.: Hoboken, 2004.
- (68) Hernandez, J. J.; Dobson, A. L.; Carberry, B. J.; Kuenstler, A. S.; Shah, P. K.; Anseth, K. S.; White, T. J.; Bowman, C. N. Controlled Degradation of Cast and 3-D Printed Photocurable Thioester Networks via Thiol-Thioester Exchange. *Macromolecules* **2022**, 55, 1376–1385.
- (69) Carberry, B. J.; Hernandez, J. J.; Dobson, A.; Bowman, C. N.; Anseth, K. S. Kinetic Analysis of Degradation in Thioester Cross-Linked Hydrogels as a Function of Thiol Concentration, pK_a , and Presentation. *Macromolecules* **2022**, *55*, 2123–2129.
- (70) Rorrer, J. E.; Troyano-Valls, C.; Beckham, G. T.; Román-Leshkov, Y. Hydrogenolysis of Polypropylene and Mixed Polyolefin Plastic Waste over Ru/C to Produce Liquid Alkanes. *ACS Sustainable Chem. Eng.* **2021**, *9*, 11661–11666.
- (71) Lipinski, B. M.; Morris, L. S.; Silberstein, M. N.; Coates, G. W. Isotactic Poly(Propylene Oxide): A Photodegradable Polymer with Strain Hardening Properties. *J. Am. Chem. Soc.* **2020**, *142*, 6800–6806.
- (72) Song, Y. K.; Hong, S. H.; Jang, M.; Han, G. M.; Jung, S. W.; Shim, W. J. Combined Effects of UV Exposure Duration and Mechanical Abrasion on Microplastic Fragmentation by Polymer Type. *Environ. Sci. Technol.* **2017**, *51*, 4368–4376.
- (73) Wang, S.; Yaszemski, M. J.; Gruetzmacher, J. A.; Lu, L. Photocrosslinked poly(ε -caprolactone fumarate) networks: Roles of crystallinity and crosslinking density in determining mechanical properties | Elsevier Enhanced Reader. *Polymer* **2008**, *49*, 5692.
- (74) Li, M.; Bijleveld, J.; Dingemans, T. J. Synthesis and Properties of Semi-crystalline Poly(decamethylene Terephthalamide) Thermosets from Reactive Side-Group Copolyamides. *Eur. Polym. J.* **2018**, *98*, 273
- (75) Gojzewski, H.; Guo, Z.; Grzelachowska, W.; Ridwan, M. G.; Hempenius, M. A.; Grijpma, D. W.; Vancso, G. J. Layer-by-Layer Printing of Photopolymers in 3D: How Weak Is the Interface? *ACS Appl. Mater. Interfaces* **2020**, *12*, 8908–8914.
- (76) FormLabs Materials Library. 2019. https://formlabs-media.formlabs.com/filer_public/ac/89/ac8963db-f54a-4cac-8fe9-fb740a7b06f1/formlabs-materials-library.pdf.

☐ Recommended by ACS

Vat Photopolymerization of Nanocellulose-Reinforced Vegetable Oil-Based Resins: Synergy in Morphology and Functionalization

Maksims Jurinovs, Sergejs Gaidukovs, et al.

MARCH 21, 2023

ACS APPLIED POLYMER MATERIALS

READ 🗹

Vat 3D Printing of Bioderivable Photoresins – Toward Sustainable and Robust Thermoplastic Parts

Kyle C. H. Chin, Andrew J. Boydston, et al.

JANUARY 20, 2023

ACS SUSTAINABLE CHEMISTRY & ENGINEERING

READ 🗹

Application of RAFT in 3D Printing: Where Are the Future Opportunities?

Ali Bagheri.

MARCH 03, 2023

MACROMOLECULES

READ 🗹

Vanillin-Based Epoxy Vitrimers: Looking at the Cystamine Hardener from a Different Perspective

Solène Guggari, Marc Guerre, et al.

APRIL 03, 2023

ACS SUSTAINABLE CHEMISTRY & ENGINEERING

READ 🗹

Get More Suggestions >